PAPER • OPEN ACCESS

Novel internal measurements of ion cyclotron frequency range fast-ion driven modes

To cite this article: N.A. Crocker *et al* 2022 *Nucl. Fusion* **62** 026023

OPEN ACCESS
IOP Publishing | International Atomic Energy Agency Nuclear Fusion

Nucl. Fusion **62** (2022) 026023 (8pp) https://doi.org/10.1088/1741-4326/ac3d6a

Novel internal measurements of ion cyclotron frequency range fast-ion driven modes

N.A. Crocker[1,*], S.X. Tang[1], K.E. Thome[2], J.B. Lestz[3], E.V. Belova[4], A. Zalzali[5], R.O. Dendy[5,6], W.A. Peebles[1], K.K. Barada[1], R. Hong[1], T.L. Rhodes[1], G. Wang[1], L. Zeng[1], T.A. Carter[1], G.H. DeGrandchamp[3], W.W. Heidbrink[3] and R.I. Pinsker[2]

[1] University of California-Los Angeles, Los Angeles, CA 90095, United States of America
[2] General Atomics, San Diego, CA 92121, United States of America
[3] University of California-Irvine, Irvine, CA 92697, United States of America
[4] Princeton Plasma Physics Laboratory, Princeton, NJ 08543, United States of America
[5] University of Warwick, Coventry, CV4 7AL, United Kingdom
[6] UK Atomic Energy Authority, Culham Centre for Fusion Energy, Abingdon, Oxfordshire OX14 3DB, United Kingdom

E-mail: ncrocker@physics.ucla.edu

Received 26 May 2021, revised 4 November 2021
Accepted for publication 25 November 2021
Published 5 January 2022

Abstract

Novel internal measurements and analysis of ion cyclotron frequency range fast-ion driven modes in DIII-D are presented. Observations, including internal density fluctuation ($\tilde{n}$) measurements obtained via Doppler backscattering, are presented for modes at low harmonics of the ion cyclotron frequency localized in the edge. The measurements indicate that these waves, identified as coherent ion cyclotron emission (ICE), have high wave number, $k_\perp \rho_{\rm fast} \gtrsim 1$, consistent with the cyclotron harmonic wave branch of the magnetoacoustic cyclotron instability, or electrostatic instability mechanisms. Measurements show extended spatial structure (at least $\sim$1/6 the minor radius). These edge ICE modes undergo amplitude modulation correlated with edge localized modes (ELM) that is qualitatively consistent with expectations for ELM-induced fast-ion transport.

Keywords: ion cyclotron emission, Doppler backscattering, energetic particles

(Some figures may appear in colour only in the online journal)

1. Introduction

Waves at harmonics of the ion cyclotron frequency ($f = lf_{ci}, |l| = 1, \ldots$) are commonly excited in fusion research plasmas by fast ions produced by neutral heating beams, acceleration by radio-frequency heating, and fusion reactions (see review in [1] and references therein). These waves, referred to as coherent ion cyclotron emission (ICE) since historically they have been detected as 'emission' from the plasma via external antennae, are thought to be attributable [1] to the magnetoacoustic cyclotron instability (MCI) [2–5], in which drive comes from Doppler-shifted cyclotron resonance between the waves and fast ions. Electrostatic instabilities have also been proposed as a potential explanation for observations of ICE at harmonics of edge values of f_{ci}. (See e.g. [4] and references therein.) These modes potentially cause transport and anomalous heating [6] and may be exploited as a tool to diagnose the fast-ion population [1].

* Author to whom any correspondence should be addressed.

This paper presents novel internal measurements and analysis of edge localized coherent ICE modes in DIII-D which exhibit amplitude modulation correlated with edge localized modes (ELMs) that may potentially advance understanding of ELM-induced fast-ion transport. Observations of internal density fluctuation ($\tilde{n}$) measurements obtained via Doppler backscattering (DBS) [7] are presented for high-k waves ($k_\perp \rho_{\rm fast} \gtrsim 1$) at low harmonics of f_{ci} localized to the edge in H-mode plasmas. (The symbol $k_\perp$ refers to the component of the wave number vector perpendicular to the equilibrium magnetic field.) These waves are identified as ICE, with features consistent with cyclotron harmonic wave branch of the MCI instability [3] or electrostatic waves (e.g. [4]). (Note that the cyclotron harmonic wave branch [8] is sometimes referred to as the ion Bernstein branch [3, 4].) The spectrum of edge ICE measured via DBS is shown to have interesting differences from the spectrum measured by edge magnetics [9], potentially explained by differences in the sensitivities of the two instruments. The structure of this paper is as follows. Section 2 describes the high frequency fluctuation diagnostics used to measure the modes, including in particular recent modifications to the DBS system that enable measurements of ICE. Section 3 presents and discusses the observations of ICE. Section 4 concludes the paper with a summary of the results.

2. High frequency fluctuation measurement technique

Two instruments are used to obtain the fluctuation measurements reported in this paper. The primary instrument is an eight channel DBS system for measuring $\tilde{n}$ [7]. This system was recently modified to expand its fluctuation measurement range up to ~75 MHz by splitting the output signal of each channel into low frequency (LF) and high frequency (HF) components using a diplexer, which are then separately digitized. The HF electronics have a combined pass band of ~16–75 MHz. The HF signals are recorded with a digitizer at 100 Msamples/sec. A DC-47 MHz anti-alias filter is used since signal components above the 50 MHz Nyquist frequency would alias to lower frequency upon digitization. The other instrument is a set of magnetic sensing loops, or antennae, positioned on the vacuum vessel wall near the plasma edge, with sensitivity to toroidal magnetic fluctuations in the 1–200 MHz range [9, 10].

The DBS system launches a beam of millimetre waves into the plasma from an antenna consisting of 8 fixed frequencies from 55–75 GHz (specifically 55, 57.5, 60, 62.5, 67.5, 70, 72.5 and 75 GHz). As illustrated in figure 1, the beam approaches from the low field side, near the midplane, obliquely incident to the plasma at a small angle to normal. The beam can be poloidally steered to control the angle of incidence. (For the results reported in this paper, the pivot point for steering is at a major radius of $R = 3.01$ m, 0.09 m below the tokamak geometric midplane. An upward tilt of ~3.0° is typically required for normal incidence, with the exact angle depending on plasma shape and position.) As millimetre waves propagate through plasma, they scatter from $\tilde{n}$ and some of the scattered waves propagate directly back to the antenna, carrying

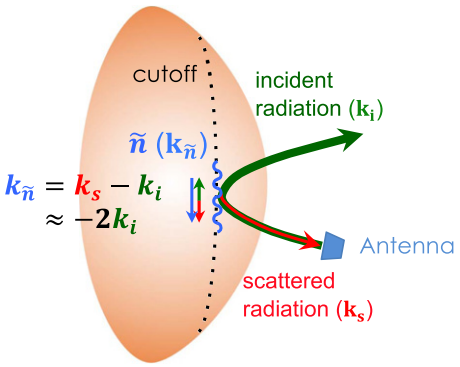

Figure 1. Illustration of DBS measurement technique.

information about $\tilde{n}$. An electronic circuit measures the amplitude (A) of the received waves and their phase (ϕ) relative to the launched waves, encoding these in 'in-phase' ($I = A\cos\phi$) and 'quadrature' ($Q = A\sin\phi$) signals. The received radiation is typically Doppler-shifted, which manifests as a continually accumulating relative phase. Results presented in this paper include analysis of the 'quadrature electric field' ($E = Ae^{i\phi} = I + iQ$) signal.

ICE $\tilde{n}$ can influence the scattered millimetre wave spectrum in at least two ways that are potentially relevant to understanding the observations presented in section 3. Scattering from a short wavelength ICE wave may contribute to the received spectrum, or a long wavelength ICE wave may modulate the spectrum of millimetre waves scattered from turbulence by displacing the plasma (and thus the turbulence) in the scattering region or by modulating the index of refraction along the beam path. Millimetre waves at different frequencies separate into individual beams upon entering the plasma, which refract poloidally along separate curved trajectories as each approaches its respective cutoff. At their closest approach to cutoff, the waves at each frequency reach a minimum in wave number and propagate approximately in the poloidal direction, as illustrated in figure 1. The ray trajectory and cutoff location, as well as wave number along the ray, can be determined from a ray tracing calculation. (For the results reported in this paper, the GENRAY ray tracing code was used [11].) The direction of launch and of the magnetic fields in the tokamak ensure that the millimeter wave number vector is approximately perpendicular to the magnetic field everywhere along the ray. Millimetre waves scatter from $\tilde{n}$ along the path according to the Bragg scattering relations, $\omega_s = \omega_i + \omega_{\tilde{n}}$ and $\mathbf{k}_s = \mathbf{k}_i + \mathbf{k}_{\tilde{n}}$, where ω and $\mathbf{k}$ correspond to frequencies and wave number vectors and the subscripts s, i and $\tilde{n}$ correspond to the incident and scattered millimetre waves and the $\tilde{n}$ causing the scattering. Since $\omega_{\tilde{n}} \ll \omega_{s,i}$, $|\mathbf{k}_s| \approx |\mathbf{k}_i|$ and the waves that scatter from $\tilde{n}$ with $\mathbf{k}_{\tilde{n}} \approx -2\mathbf{k}_i$ propagate back to the antenna, Doppler-shifted by a frequency $\omega_{\tilde{n}}$. For direct scattering from an ICE wave at frequency $\omega_{\rm ICE}$, the scattered spectrum will have peaks at $+\omega_{\rm ICE}$ or $-\omega_{\rm ICE}$, probably with unequal power in the two peaks, as illustrated in figure 2(a). The dominant peak depends on the direction of the ICE wave propagation and the amplitude is determined by the amplitude of the ICE wave. (In principle, a synthetic diagnostic model could be used to infer the ICE

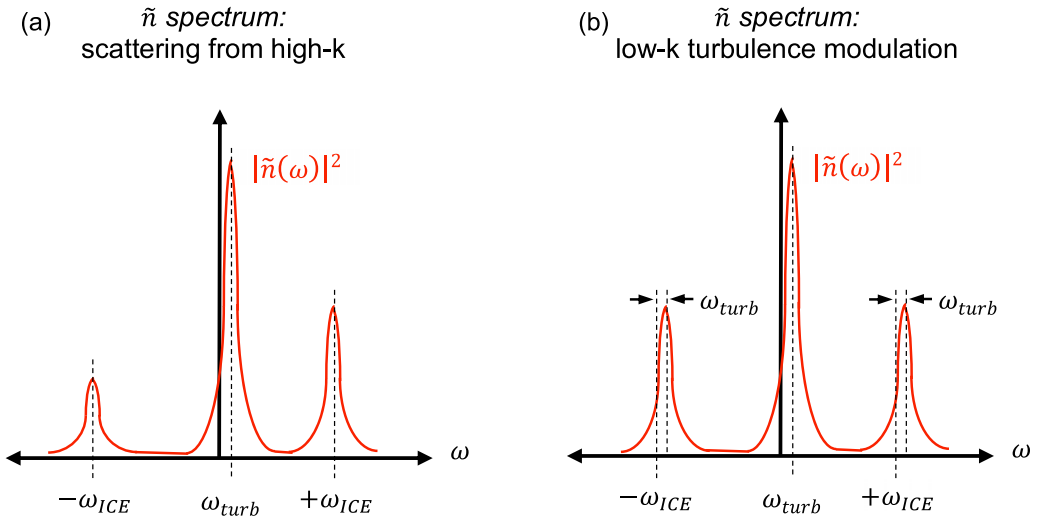

Figure 2. Illustration of DBS quadrature E ($\propto \tilde{n}$) spectra expected for (a) scattering millimetre waves from a high-k plasma wave and (b) modulation of turbulent scattering spectrum by a low-k plasma wave.

wave amplitude from the measurement, but development of this model is left to future work.) Scattering can take place anywhere along the path. The location can in principle be determined with an understanding of ICE wave dispersion characteristics since $\mathbf{k}_{\mathrm{i}}$ varies along the path. (For dispersion characteristics of electromagnetic ICE waves, see e.g. [3]. Electrostatic instabilities, e.g. [4], have also been proposed to produce ICE waves.) For modulation of the turbulent scattering spectrum, the effect of ICE $\tilde{n}$ is somewhat simpler to interpret because the spectrum reaching the antenna is expected to be dominated by scattering near cutoff. The scattering cross-section is proportional to the turbulence $\tilde{n}$ amplitude, which tends to be largest for turbulence near cutoff, since $|\mathbf{k}_{\tilde{n}}|$ reaches its smallest value there. The modulation creates equal amplitude sideband peaks in the turbulent scattering spectrum at $\omega_{\mathrm{turb}} \pm \omega_{\mathrm{ICE}}$, as illustrated in figure 2(b), where ω_{ICE} is the frequency of the ICE wave and ω_{turb} is the Doppler shift of the turbulent scattering spectrum. The sideband amplitude is determined by the ICE wave amplitude. (The Doppler shift, or peak frequency of the LF spectrum, is set by the poloidal velocity of the turbulent fluctuations causing the scattering, which is typically approximately the $E \times B$ velocity. In particular, $\omega_{\mathrm{turb}} \approx k_{\theta,\tilde{n}} v_{E\times B}$.) (The symbol $k_{\theta,\tilde{n}}$ refers to the k_θ component of the density perturbation wave number vector, where k_θ is the component in the binormal direction, perpendicular to the equilibrium magnetic field and the flux surface normal. The binormal direction is typically approximately in the poloidal direction, which motivates the use of the subscript θ.)

It may sometimes be possible to distinguish between the two cases in figure 2 via simple inspection of the measured spectra, but in cases where the Doppler shift is small it may be difficult to discern with sufficient precision whether or not the frequencies of the peaks for a given mode in the positive (f_+) and negative (f_-) frequency ranges match each other (i.e. $f_- = -f_+$). Fortunately, it possible to use a combination of bandpass filtering and coherence analysis to make a strong determination even in this case. In particular, the quadrature electric field signal can be bandpass filtered to isolate signals corresponding to the positive and negative frequency peaks of a mode. These signals take the form $E_\pm = A_\pm(t)\exp(i2\pi f_\pm t + \phi_\pm) + noise$. If $f_- \neq -f_+$, then the average of product of E_+ and E_-, $\langle E_+ E_- \rangle$, should vanish within statistical uncertainty. The sensitivity of this test will, of course, depend on details such as the amount of data used and the relative amplitude of the noise. For the measurements reported here, this analysis was used for each mode.

3. Observations of ion cyclotron harmonic range modes

Unique observations of modes with frequencies above f_{ci} ($f \sim$ 20–40 MHz $\sim$2–3 f_{ci}) test aspects of theory. Measurements of ICE $\tilde{n}$ are obtained in a variety plasma of conditions via DBS inside the plasma edge across a significant spatial range, giving mode amplitude and structure. In one instance, a high-k plasma wave at a frequency of $2f_{ci}$ is observed to extend from the plasma mid-radius to the top of the pedestal of an H-mode plasma. In another instance, spatially extended high-k plasma waves at frequencies of $2f_{ci}$ and $3f_{ci}$ are observed in the scrape-off layer (SOL) of an H-mode plasma. The plasma waves in both cases are identified as cyclotron harmonic waves excited by the MCI or electrostatic waves. In both cases, the waves exhibit amplitude modulation during ELMs consistent with stability modification by ejection of fast-ions.

Figure 3 shows DBS measurements of high-k ICE $\tilde{n}$ at $\sim 2f_{ci}$ in a deuterium H-mode plasma (shot 180203). Measurements are obtained with eight channels having cutoffs ranging from near the magnetic axis to the top of the pedestal. As shown in figure 4, at $t = 2340$ ms, the DBS system probes wave numbers $k_\theta = 2.9\ \mathrm{cm}^{-1} - 1.2\ \mathrm{cm}^{-1}$ at cutoffs at $\rho = 0.18$–0.87, where ρ is the square root of the normalized toroidal flux. (Specifically, the eight channels probe $k_\theta = 2.9$, 2.5, 2.2, 1.9, 1.5, 1.4, 1.3 and 1.2 cm^{-1} at cutoffs at $\rho = 0.18$, 0.26, 0.36, 0.48, 0.63, 0.70, 0.80 and 0.87.) As discussed in section 2, each ray reaches minimum ρ at cutoff (figures 4(a) and (b)) and the probed k_θ at cutoff is

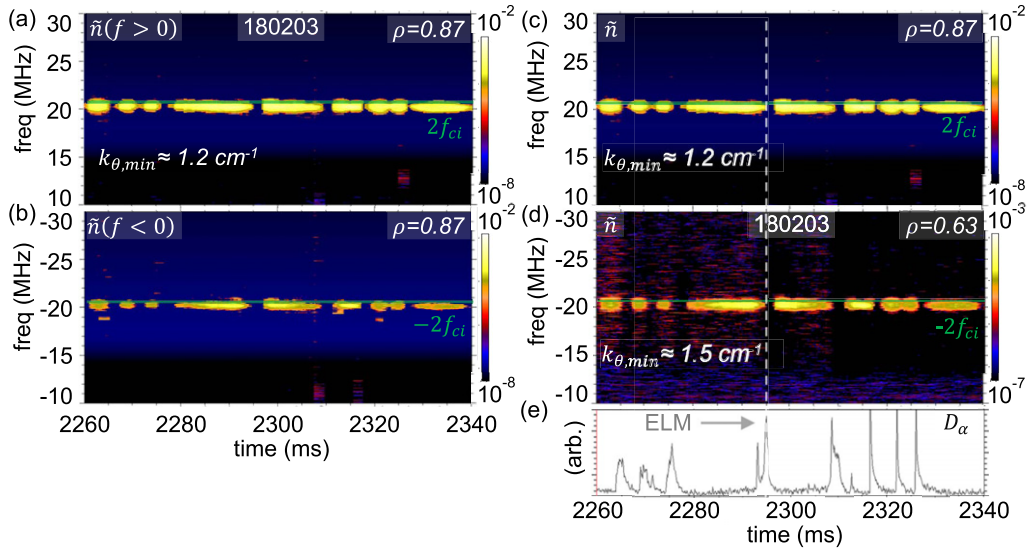

Figure 3. DBS quadrature E spectra ($\propto \tilde{n}$) at $\rho = 0.87$ for (a) positive and (b) negative frequencies stacked vertically for comparison. E spectra for (c) positive frequencies at $\rho = 0.87$ and (d) negative frequencies at $\rho = 0.63$ also stacked vertically for comparison. Background noise has been subtracted from each spectrum. All spectra are smoothed with a 2 ms $\times$ 50 kHz centered boxcar average. (e) D_α line emission. Horizontal lines in (a)–(d) illustrate average value of $2f_{ci}$ ($\sim$20.9 MHz) for $\rho = 0.63$–0.87 in the low field side midplane. Vertical line in (c)–(e) is a guide to illustrate the correlation of D_α spikes with $\tilde{n}$ suppression. The minimum $k_\perp$ probed ($k_{\theta,\min}$) for the beam that reaches cutoff at $\rho = 0.87$ is shown in (a) and (c), while (d) shows $k_{\theta,\min}$ for the beam that reaches cutoff at $\rho = 0.63$.

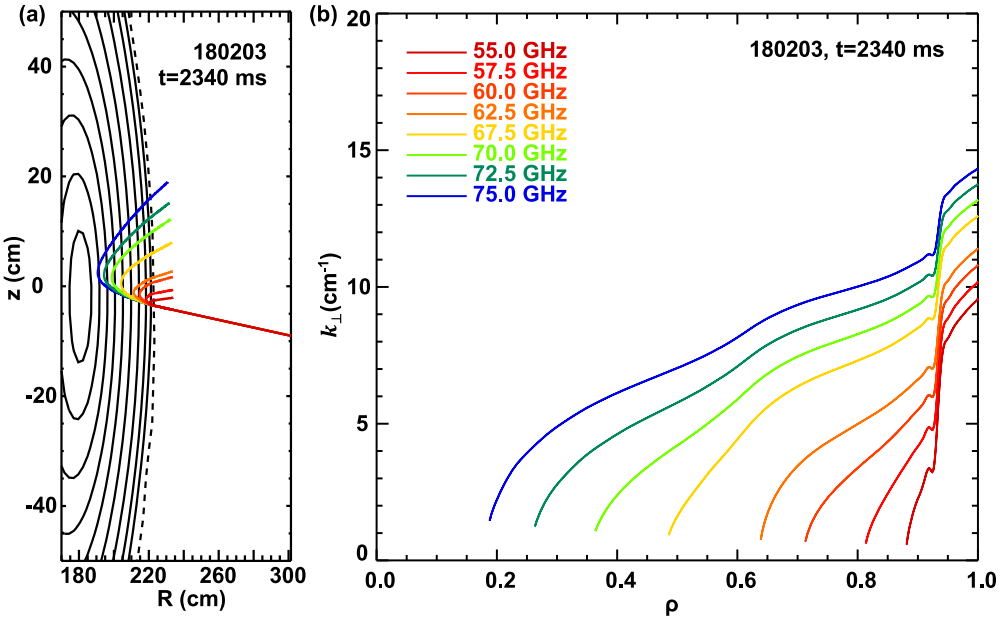

Figure 4. (a) Colored lines show trajectories for DBS millimetre wave rays in R–Z plane calculated using GENRAY ray tracing. Colors correspond to millimetre wave frequencies shown in legend of panel (b); solid contours are flux surfaces for $\rho = 0.1, 0.2, \ldots, 0.9$; dashed contour is last closed flux surface ($\rho = 1$). (b) Value of $k_\perp$ vs ρ for millimetre waves at each frequency of DBS.

related to the millimetre wave $k_\perp$ (figure 4(b)) by $k_\theta = 2k_\perp$. During the period shown, the plasma has current $I_P = 820$ kA, and electron temperature, electron density, safety factor and magnetic field at the magnetic axis of $T_{e0} = 3$ keV, $n_{e0} = 7.0 \times 10^{19}$ m^{-3}, $q_0 = 4.4$ and $B_0 \approx 1.59$ T, respectively. (The magnetic field is actually slowly ramping down, decreasing $<2\%$ within the period shown in figure 3, and $\sim$18% over the period $t = 1400$–3500 ms.) The magnetic axis is at $R_0 = 1.81$ m and the last closed flux surface outer boundary is $R_{\text{midout}} = 2.23$ m. (These locations remain approximately fixed over most of the period $t = 1400$–3500 ms.) Equilibrium reconstruction is performed using external magnetic measurements, as well as internal magnetic field pitch measurements from motional Stark effect spectroscopy [12]. The toroidal magnetic field is oriented in the same direction as the plasma current. Deuterium neutral beam power varies between $P_{\text{NB}} \sim 5$ MW and 9 MW as various beams are modulated on and off, including the more tangential ($R_{\text{TAN}} = 1.15$ m) on-axis and more perpendicular ($R_{\text{TAN}} = 0.76$ m) on-axis beams, as well as off-axis beams. The on-

axis beams, in particular, are rapidly switched on and off with on- and off-times as short at 10 ms, while the off-axis beams remain on except for occasional short (∼10–20 ms) off periods. All beams inject in the plasma current direction, with $E_{\rm beam} = 73$–81 keV. The fast-ion gyro-radius is $\rho_{\rm fast} \sim 3$–4 cm for fast ions deposited on the low field side by the on-axis beams. The off-axis beamlines were tilted, leading to more parallel injection and smaller $\rho_{\rm fast}$ than the on-axis beams because of the direction of the toroidal field [13].

The high-k ICE in figure 3 has features indicating that the peaks at $|f| \sim 2f_{ci}$ in the spectra are the result of the millimetre waves scattering from a high-k plasma wave. In particular, figures 3(a) and (b) show the positive and negative frequency ranges of the DBS quadrature E spectra ($\propto \tilde{n}$) for millimetre waves with a cutoff at $\rho = 0.87$. Both feature a peak at $|f| \sim$ 20.5 MHz. This is similar to the value of $2f_{ci}$ (∼20.7 MHz) at $\rho = 0.87$ on the low field side midplane, and it matches $2f_{ci}$ just outside $\rho = 1$. (Notably, this peak appears in the spectrum throughout most of the time period $t = 1400$–3500 ms during which $B_{\rm T}$ ramps down, changing frequency strictly in proportion to $B_{\rm T}$. This proportionality ensures that the mode frequency matches $2f_{ci}$ very close to the boundary during the entire ramp.) The frequencies of the peaks in the positive (f_+) and negative (f_-) frequency ranges match each other ($f_- = -f_+$). Furthermore, the amplitude of the peak at positive frequency is greater than that at negative frequency. This agreement in frequency is expected for scattering from a high-k plasma wave and the asymmetric distribution of power is also consistent. (For the alternative case where the peaks were turbulence sidebands caused by modulation of the millimeter waves by a long wavelength plasma wave, the peak in the negative frequency range would be expected to have frequency $f_- = 2f_{\rm turb} - f_+$, where $f_{\rm turb} \sim 100$–300 kHz is the Doppler shift observed in the LF spectrum for this plasma, and the two peaks would have equal power.) The millimetre wave beam probes a minimum k at cutoff of $k_\theta = 1.2$ cm^{-1}, so the plasma wave has $k_\perp \geqslant 1.2$ cm^{-1}. The high k and near-harmonic frequency of the plasma wave causing the scattering are consistent with a cyclotron harmonic wave driven by the MCI instability or an electrostatic wave. The MCI instability involves excitation of electromagnetic waves on the fast Alfvén and cyclotron harmonic wave branches [3]. A fast Alfvén wave would have $k = \omega/v_{\rm A} \sim 0.4$ cm^{-1} for a 20.5 MHz mode ($n_{\rm e} \sim 3.75 \times 10^{19}$ m^{-3} and $v_{\rm A} \sim 3.4 \times 10^6$ m s^{-1} at $\rho = 0.87$), which is sufficiently low that the mode cannot be a fast Alfvén wave. However, the value of $k_\perp$ for the cyclotron harmonic wave is expected to be significantly larger ($k_\perp \rho_{\rm fast} \gtrsim 1$). The high k may also be consistent with an electrostatic wave (e.g. [4]). Distinguishing between these possibilities will require careful consideration of what each theory predicts for these conditions.

The ∼20.5 MHz mode is radially extended and exhibits amplitude modulation correlated with ELM activity. Peaks at the same frequency of $|f| \sim 20.5$ MHz are visible in the positive and/or negative frequency ranges of the spectra of the four outermost channels, which probe $k_\theta = 1.5$ cm^{-1}–1.2 cm^{-1} at cutoffs at $\rho = 0.63$–0.87. Figures 3(c) and (d) show examples at $\rho = 0.87$ and 0.63. (Note that the negative frequency range of the spectrum is shown for $\rho = 0.63$ in figure 3(d) because the power distribution at $|f| \sim 20.5$ MHz is very asymmetric and a peak at +20.5 MHz is difficult to discern above the background level, in keeping with the mode being high-k.) These cutoffs span a radial distance of $\Delta R \sim 7$ cm $\approx a/6$, (using $a = R_{\rm midout} - R_0$), or $\Delta R \sim 2\rho_{\rm fast}$. However, the radial extent of the mode is potentially greater. While the four innermost channels do not see the mode, placing a limit on the extent of the mode toward the magnetic axis, there are no channels closer to the edge to show the limit of the mode's radial extent in that direction. A radially extended mode would be expected for the MCI instability since emission from the resonant fast ions can propagate radially. It should be noted that in this scenario the location where the emission originates could be near, but not at, the location where the frequency matches the harmonic because of a non-vanishing Doppler shift contribution to resonance. As can be seen in figure 3(e), the mode amplitude is transiently suppressed during spikes in D_α emission corresponding to ELMs. Any candidate instability must be able explain the radial extent and amplitude sensitivity to ELMs. The amplitude of the mode is not obviously correlated over the long period of the $B_{\rm T}$ ramp with the modulation of any the beams, including in particular the on-axis beams, which are rapidly modulated.

Figure 5 shows DBS measurements of high-k ICE $\tilde{n}$ at ∼$2f_{ci}$ and ∼$3f_{ci}$ in the SOL of an H-mode deuterium plasma (shot 179437). For the time period shown, the plasma has $T_{\rm e0} = 6.5$ keV, $q_0 = 0.7$ and $B_0 = 2.0$ T. Plasma current is $I_{\rm P} = 1.5$ MA, while electron density ramps up from $n_{\rm e0} = 5.5 \times 10^{19}$ m^{-3} at $t = 1650$ ms to 6.5×10^{19} m^{-3} at $t = 1880$ ms and then $I_{\rm P}$ ramps quickly down as plasma termination begins, passing through 1.35 MA by $t = 1900$ ms. The deuterium neutral beam power is initially $P_{\rm NB} = 6.5$ MW and then steps down to 4.5 MW at $t = 1700$ ms, finally shutting off at $t = 1880$ ms. All beams are injecting in the plasma current direction, opposite the direction of the toroidal field, with energies of $E_{\rm beam} = 71$–79 keV and a fast-ion gyro-radius of $\rho_{\rm fast} \sim 2$ cm for fast ions deposited on the low field side. Some on-axis beams are rapidly modulated off and on, while others remain on until $t = 1880$ ms. The off-axis beams are modulated more slowly before $t = 1700$ ms, completely shutting off afterwards (contributing to the step-down in total power). Notably, while the beams are all off after $t = 1880$ ms, the total D–D neutron rate drops only by a factor of ∼2 by the end of the time window in figure 5, $t = 1900$ ms. The magnetic axis is $R_0 = 1.73$ m and the last closed flux surface outer boundary is $R_{\rm midout} = 2.27$ m. Equilibrium reconstruction is performed using external magnetic measurements [14].

The high-k ICE in figure 5 has features indicating that the peaks at $|f| \sim 2f_{ci}$ and $3f_{ci}$ in the spectra are the result of millimetre waves scattering from a high-k plasma wave. In particular, figures 5(a) and (b) show the positive and negative frequency ranges of the DBS quadrature E spectra ($\propto \tilde{n}$) of millimetre waves with a cutoff at $\rho = 1.06$, in the SOL. (For $\rho > 1$, ρ is the square root of the normalized poloidal flux.) Both feature peaks at $f = 23.2$ and 35.3 MHz, approximately matching $2f_{ci}$ and $3f_{ci}$ in the vicinity of the cutoffs ($f_{ci} = 11.8$ MHz). As in the previous example (figure 3), the

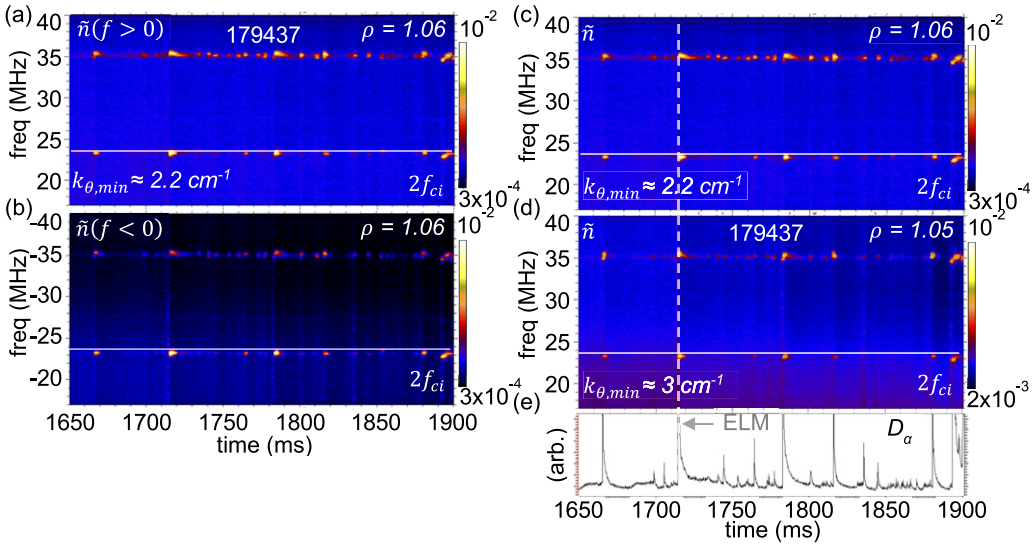

Figure 5. DBS quadrature E spectra ($\propto \tilde{n}$) at $\rho = 1.06$ for (a) positive and (b) negative frequency stacked vertically for comparison. E spectra for positive frequencies at (c) ρ =1.06 and (d) ρ =1.05 also stacked vertically for comparison. All spectra are smoothed with a 2 ms × 50 kHz centered boxcar average. (e) D_α line emission. Horizontal lines in (a)–(d) illustrate average value of $2f_{ci}$ (∼23.6 MHz) for $\rho = 1.05$–1.06 in the low field side midplane. Vertical line in (c)–(e) is a guide to illustrate the correlation of D_α spikes with $\tilde{n}$ excitation. The minimum $k_\perp$ probed ($k_{\theta,\mathrm{min}}$) for the beam that is cutoff at $\rho = 1.06$ is shown in (a) and (c), while (d) shows $k_{\theta,\mathrm{min}}$ for the beam that is cutoff at $\rho = 1.05$.

identical positive and negative frequencies implies that this is a high-k wave, not millimetre waves scattered by turbulence and the asymmetry in amplitude is consistent with this interpretation. (The Doppler shift of the turbulent spectrum is $f_{\mathrm{turb}} \sim 100$ kHz for this case.) The millimetre wave beam probes a minimum k at cutoff of $k_\theta = 2.2$ cm^{-1}, so the plasma wave has $k \geqslant 2.2$ cm^{-1}. The high-k and near-harmonic frequency of the plasma wave causing the scattering are consistent with a cyclotron harmonic wave or electrostatic wave. The value of k is sufficiently high that it cannot be a fast Alfvén wave, which would have $k = \omega/v_{\mathrm{A}} \sim 0.1$ cm^{-1} for the 23.5 MHz peak ($n_{\mathrm{e}} \sim 4 \times 10^{18}$ m^{-3}, and $v_{\mathrm{A}} \sim 12 \times 10^6$ m s^{-1}), too small for the probed k.

These modes at $|f| \sim 2f_{ci}$ and $3f_{ci}$ are spatially extended and exhibit amplitude modulation correlated with ELM activity. In particular, figures 5(c) and (d) show DBS quadrature E spectra ($\propto \tilde{n}$) from millimetre-wave beams probing k_θ = 2.2 cm^{-1} and $k_\theta = 3.0$ cm^{-1} at cutoffs in the SOL at $\rho = 1.06$ and 1.05. These cutoffs are separated by $\Delta R \sim 3/4$ cm. Only two channels are available for measurements in this case, so the full spatial extent cannot be determined. Figure 5(e) show that, in contrast to the previous example, ELMs transiently enhance the emission for these SOL measurements. The emission is not obviously correlated with the modulation of any the beams.

Simultaneous measurements of $\tilde{b}$ with the toroidal loop on the vacuum vessel wall show distinct differences from the spectrum of high-k ICE modes observed by DBS in figure 5. Figures 6(a) and (b) show time slices of the spectra at t = 1716.5 ms from figures 5(c) and (d), while figure 6(c) shows the $\tilde{b}$ spectrum at the wall from the same time. The $\tilde{b}$ spectrum exhibits peaks at $f \sim 2f_{ci}$ and $3f_{ci}$ for a value of f_{ci} in the edge, as does the DBS spectrum, but the frequencies of those peaks are lower than those in the DBS spectrum by $\sim\frac{1}{2}$ MHz. (This difference cannot be attributed to differences

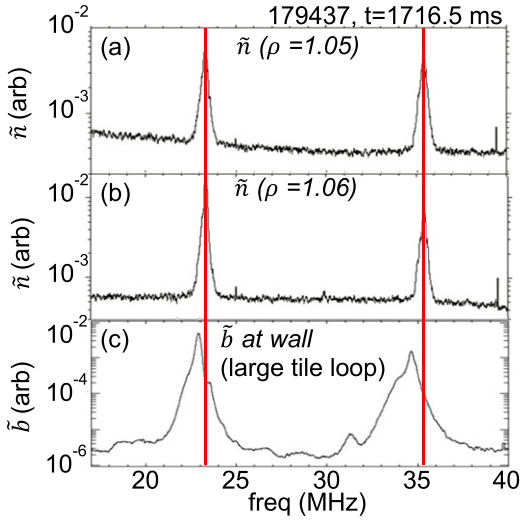

Figure 6. DBS quadrature E spectra ($\propto \tilde{n}$) at (a) ρ =1.05 and (b) ρ =1.06 at t = 1716.5 ms in shot 179437. (c) Magnetic spectrum ($\tilde{b}$) from tile loop on wall for the same time. Peaks of the $\tilde{n}$ spectra match each other in frequency, but not those of $\tilde{b}$ spectrum. Vertical lines highlight these agreements and differences.

in the time bases for the magnetic and DBS diagnostics. Testing with a crystal oscillator showed that the time bases differ by less than 10 Hz.) In contrast, the peaks in both DBS spectra match each other, in keeping with the spatially extended nature of the mode. The explanation for this difference is under investigation; one possible explanation is that, owing to wave attenuation in the SOL, the tile loops are more sensitive to low-k waves than to the high-k waves detected by DBS. Fast Alfvén waves, which would have a long wavelength of $\lambda = v_{\mathrm{A}}/f \gtrsim 30$ cm (using $f \lesssim 35$ MHz, $v_{\mathrm{A}} \gtrsim 12 \times 10^6$ m s^{-1}), may potentially more readily penetrate across the vacuum to the tile loop.

The high-k edge ICE modes depicted in figures 3 and 5 both show a sensitivity to ELM activity that is potentially explained by fast ion ejection by ELMs [15] if the modes are cyclotron harmonic waves driven by the MCI. The pedestal-top mode in figure 3 exhibits sudden transient drops in amplitude during spikes in D_α line emission (figure 3(e)), while the SOL modes in figure 5 are in contrast transiently destabilized when D_α spikes (figure 5(e)) due to ELMs. (A transient excitation of edge ICE by ELMS in DIII-D was also reported in [16].) The transient stabilization of the pedestal-top mode is consistent with a transient depletion of fast ions responsible for exciting the mode [17]. The transient excitation of the SOL modes is consistent with the passage of ejected fast ions transiently providing drive for the modes [18]. Unfortunately, it is not possible from existing data to discriminate between fast ions from beams and fusion products as the source of drive. ICE observed by the toroidal loops on the vacuum vessel wall has been shown in other cases in DIII-D to be excited by ions from beams based on an observed correlation between modulation of beam power and ICE amplitude [16]. Although there is some modulation of some beams for the two cases, there is no obvious correlation of the emission with the beam modulation. Following the reasoning in [16], this would argue against at least some beams as the source of the fast ions exciting the ICE, but not all. The final burst of mode activity after $t \sim 1890$ ms in figure 5 is interesting since it occurs $\sim$10 ms after all beams have shut off and persists for $\sim$10 ms. The total D–D neutron rate has dropped by a factor of $\sim$2 by $t \sim 1900$ ms, so there clearly remains a significant population of fast ions throughout this period, as well as continued production of D–D fusion products, to be transported by the associated ELM. In addition to causing fast-ion transport, ELMs also cause abrupt changes in edge density and temperature profiles which must also be accounted for. These profile changes could play a role in the stability and characteristics of an edge-localized ion cyclotron harmonic wave driven by fast ions. They could also destabilize electrostatic waves, potentially offering an alternate explanation these observations. Examples include ion-cyclotron drift waves [19] or drift-cyclotron loss-cone waves [20]. Of course, the stability of such gradient driven electrostatic instabilities may potentially be altered by the presence an anisotropic fast-ion population. Also, the sudden ejection of fast ions may indirectly affect wave stability by, for instance, transiently changing the local plasma velocity profile [21]. Further analysis and modelling will be required to evaluate these possibilities.

4. Conclusions

In conclusion, novel measurements are presented for high wave number $\left(k_\perp \rho_{\mathrm{fast}} \gtrsim 1\right)$ ICE in the edge of DIII-D. These measurements are shown to be consistent with the cyclotron harmonic wave branch of the MCI instability or an electrostatic instability and not consistent with fast Alfvén waves, which would have much lower wave number. Measurements of ICE spatial structure show significant spatial extent (at least $\sim$1/6 the minor radius). These observations of ICE may potentially advance our understanding of ELM-induced fast-ion transport. Comparisons of experiment with theory show areas of agreement, building confidence in its predictive power. These results strengthen the physics basis for predicting fast-ion driven mode activity and concomitant fast-ion transport in future burning plasmas.

Disclaimer

Acknowledgments

This material is based upon work supported by the U.S. Department of Energy, Office of Science, Office of Fusion Energy Sciences, using the DIII-D National Fusion Facility, a DOE Office of Science user facility, under Award(s) DE-FC02-04ER54698. This work was also supported in part by the US Department of Energy under Grant and Contract Nos. DE-FG02-99ER54527, DE-SC0011810, DE-SC0019352, DE-SC0020337, and DE-AC02-09CH11466. It was supported in part from the RCUK Energy Programme Grant No. EP/T012250/1 and carried out in part within the framework of the EUROfusion Consortium, receiving funding from the Euratom Research and Training Programme 2014–2018 and 2019–2020 under Grant agreement No. 633053.

ORCID iDs

N.A. Crocker https://orcid.org/0000-0003-2379-5814
S.X. Tang https://orcid.org/0000-0001-7030-5473
K.E. Thome https://orcid.org/0000-0002-4801-3922
J.B. Lestz https://orcid.org/0000-0002-6975-1537
E.V. Belova https://orcid.org/0000-0002-1525-1027
K.K. Barada https://orcid.org/0000-0001-7724-8491
R. Hong https://orcid.org/0000-0003-4750-8015
T.L. Rhodes https://orcid.org/0000-0002-8311-4892
G. Wang https://orcid.org/0000-0002-2573-9827
L. Zeng https://orcid.org/0000-0001-5856-3912
T.A. Carter https://orcid.org/0000-0002-5741-0495
G.H. DeGrandchamp https://orcid.org/0000-0002-1363-9570
W.W. Heidbrink https://orcid.org/0000-0002-6942-8043
R.I. Pinsker https://orcid.org/0000-0003-2683-9480

References

[1] McClements K.G., D'Inca R., Dendy R.O., Carbajal L., Chapman S.C., Cook J.W.S., Harvey R.W., Heidbrink W.W. and Pinches S.D. 2015 Fast particle-driven ion cyclotron emission (ICE) in tokamak plasmas and the case for an ICE diagnostic in ITER *Nucl. Fusion* **55** 043013

[2] Belikov V.S. and Kolesnichenko I.I. 1976 Magnetoacoustic cyclotron instability in a thermonuclear plasma *Sov. Phys. Tech. Phys.* **20** 1146–51

[3] Dendy R.O., Lashmore-Davies C.N., McClements K.G. and Cottrell G.A. 1994 The excitation of obliquely propagating fast Alfvén waves at fusion ion cyclotron harmonics *Phys. Plasmas* **1** 1918–28

[4] Dendy R.O., McClements K.G., Lashmore-Davies C.N., Majeski R. and Cauffman S. 1994 A mechanism for beam-driven excitation of ion cyclotron harmonic waves in the Tokamak fusion test reactor *Phys. Plasmas* **1** 3407–13

[5] Gorelenkov N.N. 2016 Energetic particle-driven compressional Alfvén eigenmodes and prospects for ion cyclotron emission studies in fusion plasmas *New J. Phys.* **18** 105010

[6] Kolesnichenko Y.I., Tykhyy A.V. and White R.B. 2020 Spatial channeling in toroidal plasmas: overview and new results *Nucl. Fusion* **60** 112006

[7] Peebles W.A., Rhodes T.L., Hillesheim J.C., Zeng L. and Wannberg C. 2010 A novel, multichannel, comb-frequency Doppler backscatter system *Rev. Sci. Instrum.* **81** 10D902

[8] Chapman B., Dendy R.O., Chapman S.C., McClements K.G., Yun G.S., Thatipamula S.G. and Kim M.H. 2019 Interpretation of suprathermal emission at deuteron cyclotron harmonics from deuterium plasmas heated by neutral beam injection in the KSTAR tokamak *Nucl. Fusion* **59** 106021

[9] Thome K.E., Pace D.C., Pinsker R.I., Meneghini O., del Castillo C.A. and Zhu Y. 2018 Radio frequency measurements of energetic-particle-driven emission using the ion cyclotron emission diagnostic on the DIII-D tokamak *Rev. Sci. Instrum.* **89** 10I102

[10] Degrandchamp G.H., Thome K.E., Heidbrink W.W., Holmes I. and Pinsker R.I. 2021 Upgrades to the ion cyclotron emission diagnostic on the DIII-D tokamak *Rev. Sci. Instrum.* **92** 033543

[11] Smirnov A.P., Harvey R.W. and Kupfer K. 1994 A general ray tracing code GENRAY *Bull. Am. Phys. Soc.* **39** 1626

[12] Holcomb C.T., Makowski M.A., Allen S.L., Meyer W.H. and van Zeeland M.A. 2008 Overview of equilibrium reconstruction on DIII-D using new measurements from an expanded motional Stark effect diagnostic *Rev. Sci. Instrum.* **79** 10F518

[13] Murakami M. *et al* 2009 Off-axis neutral beam current drive for advanced scenario development in DIII-D *Nucl. Fusion* **49** 065031

[14] Lao L.L., John H.E.S., Peng Q., Ferron J.R., Strait E.J., Taylor T.S., Meyer W.H., Zhang C. and You K.I. 2005 MHD equilibrium reconstruction in the DIII-D tokamak *Fusion Sci. Technol.* **48** 968–77

[15] García-Muñoz M. *et al* 2013 Fast-ion redistribution and loss due to edge perturbations in the ASDEX Upgrade, DIII-D and KSTAR tokamaks *Nucl. Fusion* **53** 123008

[16] Thome K.E., Pace D.C., Pinsker R.I., van Zeeland M.A., Heidbrink W.W. and Austin M.E. 2019 Central ion cyclotron emission in the DIII-D tokamak *Nucl. Fusion* **59** 086011

[17] Cottrell G.A. *et al* 1993 Ion cyclotron emission measurements during JET deuterium–tritium experiments *Nucl. Fusion* **33** 1365–87

[18] Thatipamula S.G., Yun G.S., Leem J., Park H.K., Kim K.W., Akiyama T. and Lee S.G. 2016 Dynamic spectra of radio frequency bursts associated with edge-localized modes *Plasma Phys. Control. Fusion* **58** 065003

[19] Hendel H.W. and Yamada M. 1974 Identification of ion-cyclotron drift instability with discrete and continuous spectra *Phys. Rev. Lett.* **33** 1076–9

[20] Farmer W.A. and Morales G.J. 2016 Stability of drift-cyclotron loss-cone waves in H-mode plasmas *Nucl. Fusion* **56** 064003

[21] Ganguli G., Lee Y.C. and Palmadesso P. 1985 Electrostatic ion-cyclotron instability caused by a nonuniform electric field perpendicular to the external magnetic field *Phys. Fluids* **28** 761–3